FigureS1 related to Figure2

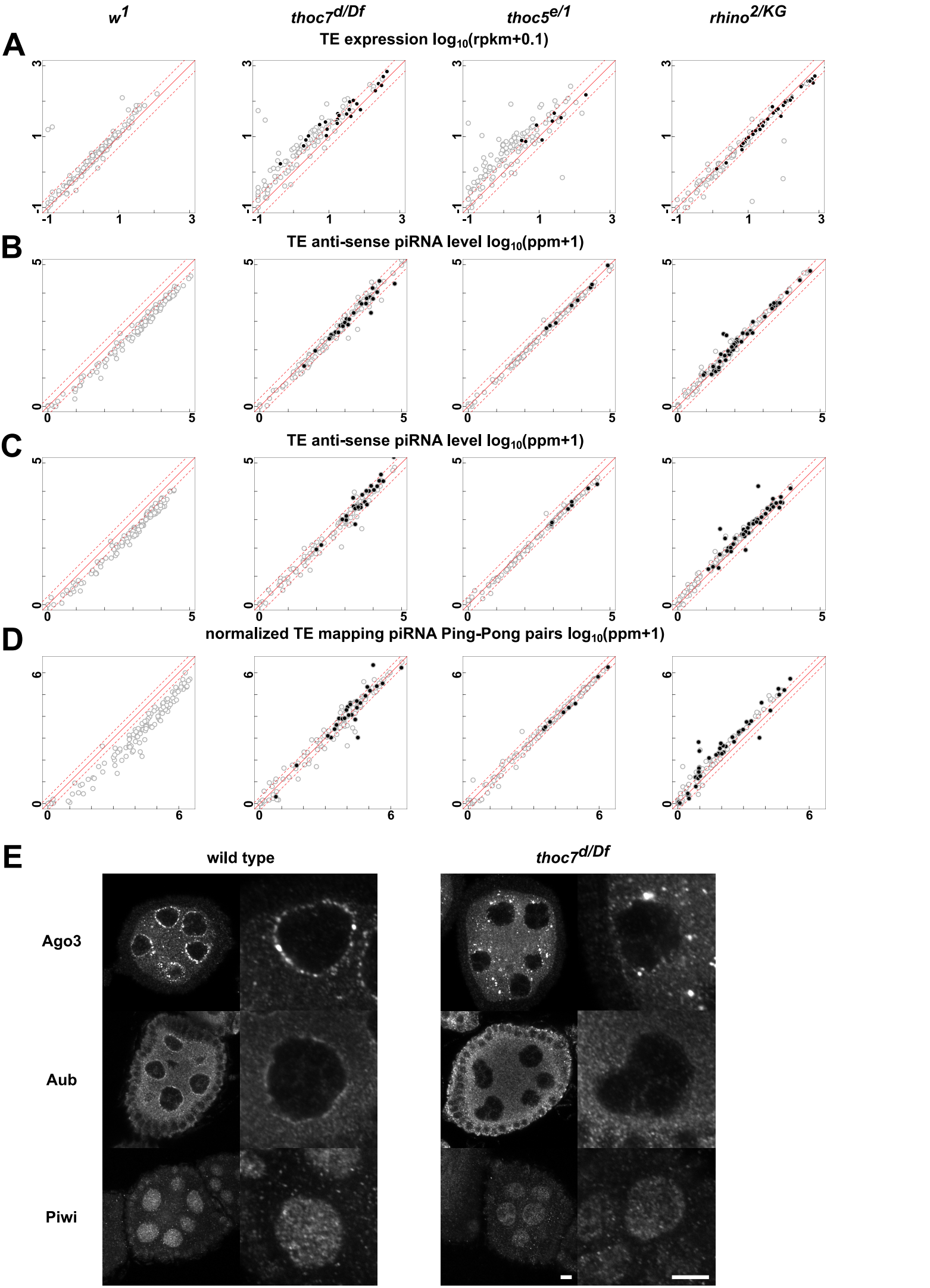

Figure S1: Reproducibility of deep sequencing data between replicates and PIWI proteins localization in *thoc7* mutants, related to Figure2.

A, B and C. Scatter plots compare the transposon expression (A), transposon mapping antisense small RNA abundance (B), sense small RNA abundance (C) and normalized ping-pong pairs (D) between two biological replicates in the indicated genotypes. Solid circles highlight the overexpressed transposon in the mutants comparing to w^1.

F. Immunofluorescence images of stage six egg chamber and single nucleus stained with indicated PIWI proteins (Aub, Ago3 and Piwi). Scale bar: 5μm.

Figure S2 related to Figure 2

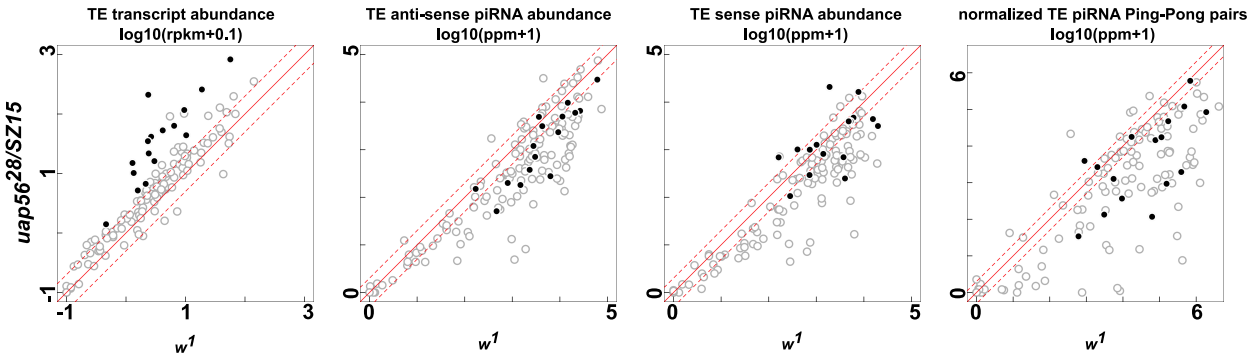

Figure S2. Transposon expression, antisense and sense piRNA abundance, and ping-pong signature in *uap56* mutants, related to Figure2.

UAP56 function with THO in the TREX complex. However, the hypomorphic *uap56* allelic combination that disrupts transposon silencing, produces more pronounced reductions in transposon mapping antisense piRNA and ping-pong pairs than *thoc7* null allele (compare second and fourth panels with Figure 2B and D).

FigureS3 related to Figure 3

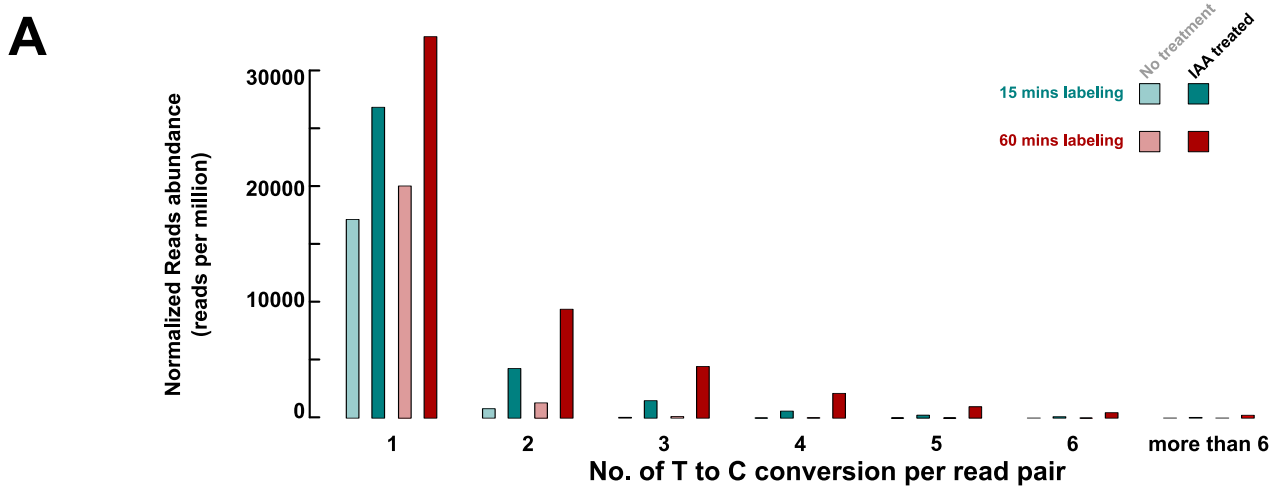

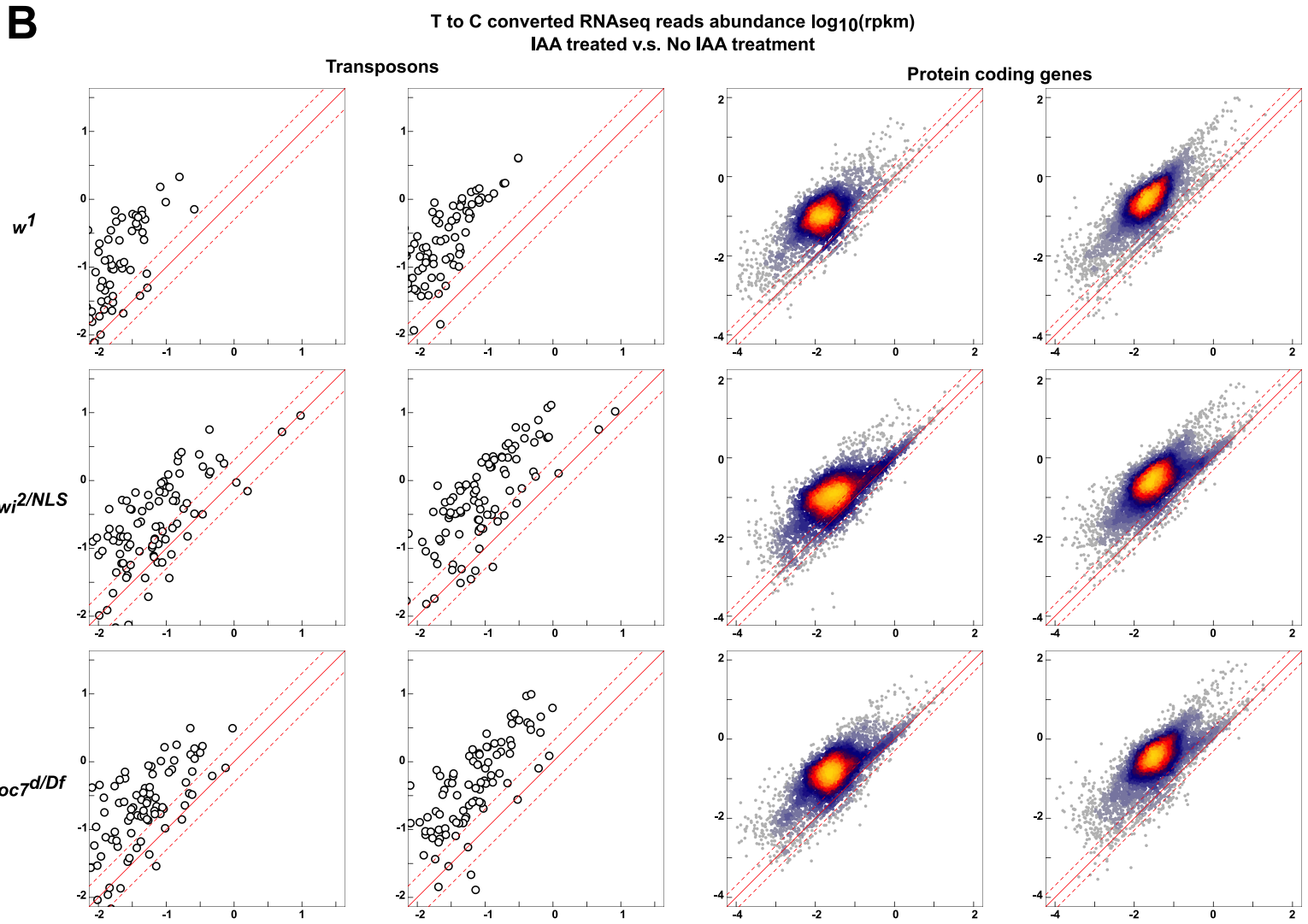

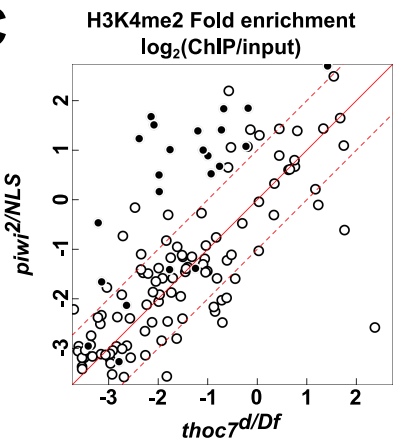

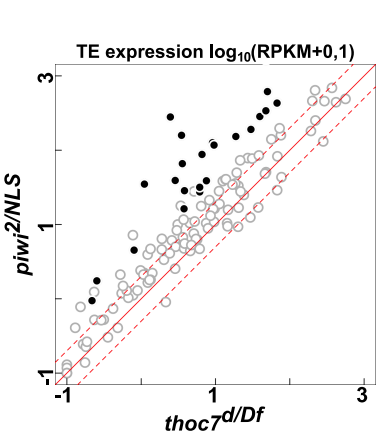

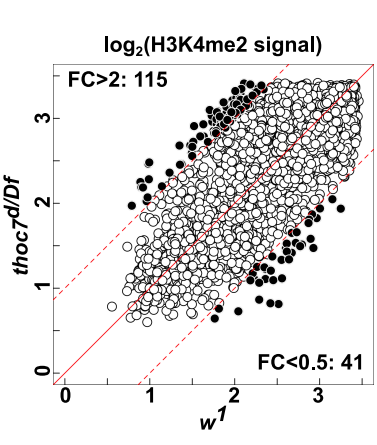

Figure S3: SLAM-seq labels nascent transcripts, related to Figure3.

A. Sequencing depth normalized quantification of RNA-seq reads with indicated number of “T to C” conversion *per* read pair in two time points of labeling (15mins and 60mins) and two conditions of chemical treatment (no treatment and IAA treated).

B. Scatter plots comparing abundance of transposons (left two columns) and protein-coding genes (right two columns) mapping RNA-seq reads with at least TWO “T to C” conversions *per* read pair normalized to sequencing depth between IAA treated RNA sample and no treatment control for indicated genotypes and labeling time points.

C. Scatter plot compares fold-enrichment of H3K4me2 ChIP-seq signals (ChIP/input) mapping to the first two kilo-bases of transposon consensus between *piwi*$^{2/NLS}$ and *thoc7*$^{d/}$*Df*. The solid circles represent transposons overexpressed in *piwi*$^{2/NLS}$ comparing to *thoc7*$^{d/}$*Df* (FC > 2, FDR<0.01).

D. Scatter plot compares transposon expression between *piwi*$^{2/NLS}$ and *thoc7*$^{d/}$*Df*. The solid circles represent transposons overexpressed in *piwi*$^{2/NLS}$ comparing to *thoc7*$^{d/}$*Df*.

E. Scatter plot comparing ChIP-seq signal of annotated H3K4me2 peaks mapping to protein-coding gene promoters between *thoc7*$^{d/}$*Df* and *w*^{1}.

Figure S4 related to Figure 4

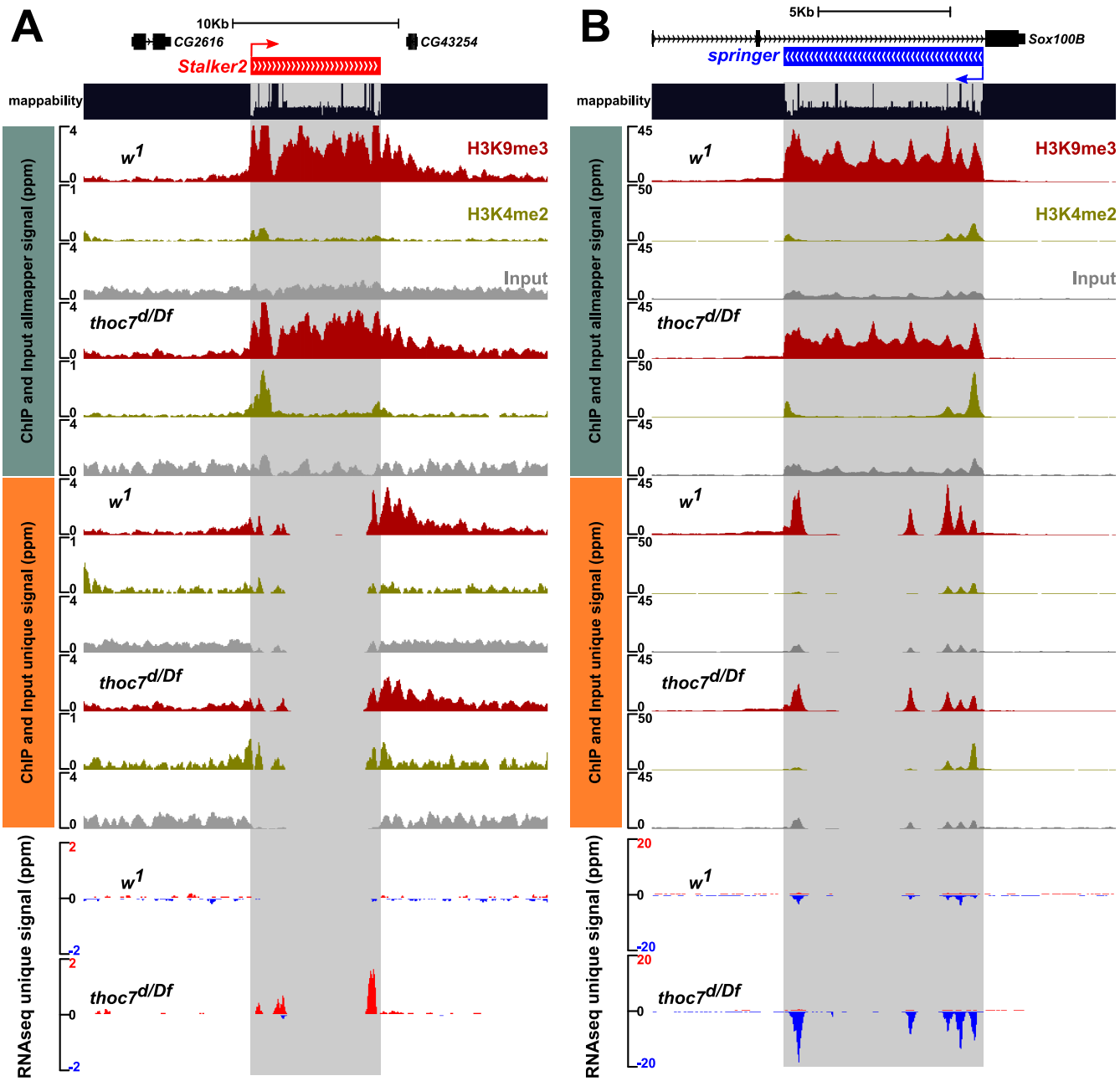

Figure S4: Mutations in *thoc7* do not disrupt H3K9me3 modification at transcriptionally activated transposon insertions present in the reference genome. Related to Figure 4.

Genome browser views of *Stalker2* and *Springer* transposon insertions that are present in both the reference genome and *thoc7* mutants, allowing direct mapping of long RNAseq, H3K9me3 and H3K4me2 ChIPseq to unique polypmorhisms. The *thoc7* mutation increases steady state transcript levels and H3K4me2 at both insertions, but does not reduce H3K9me3. All mapping and unique mapping tracks are shown for the ChIP data, with input in gray. Unique signal is shown in the RNAseq tracks (bottom panels).

FigureS5 related to Figure 5

A

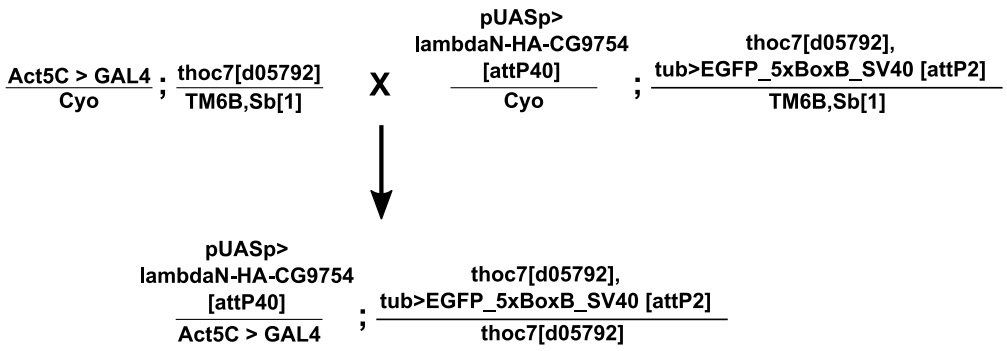

B

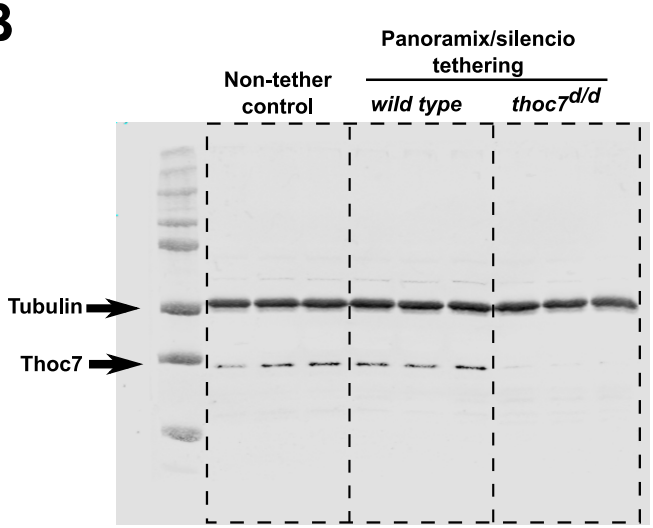

Figure S5: Reporter transgene analysis of *thoc7* function in Panx-dependent silencing. Related to Figure 5.

A. Genetic crosses used to generate ovaries carrying the reporter transgene (tub>EGFP_5xBoxB_SV40 [attP2]), lambda-tagged Panx (pUASp.lambdaN-HA-CG9754 [attP40), and the transcriptional driver (Act5C>Gal4), in the *thoc7* mutant background (thoc7[d05792]). CG9754 is the original designation for *panx*. CyO is a second chromosome balancer carrying a dominant curly wing marker, and TM6B, Sb is a third chromosome balancer carrying a dominant stubby bristle marker. The experimental flies are identified by the absence of these dominant markers. B. Western blots for Thoc7 protein were used to confirm the *thoc7* mutant genotype, indicated by the absence of protein. Three biological replicates were assayed for each experimental condition. Blotting for Tubulin served as a loading control.

Figure S6 related to Figure7

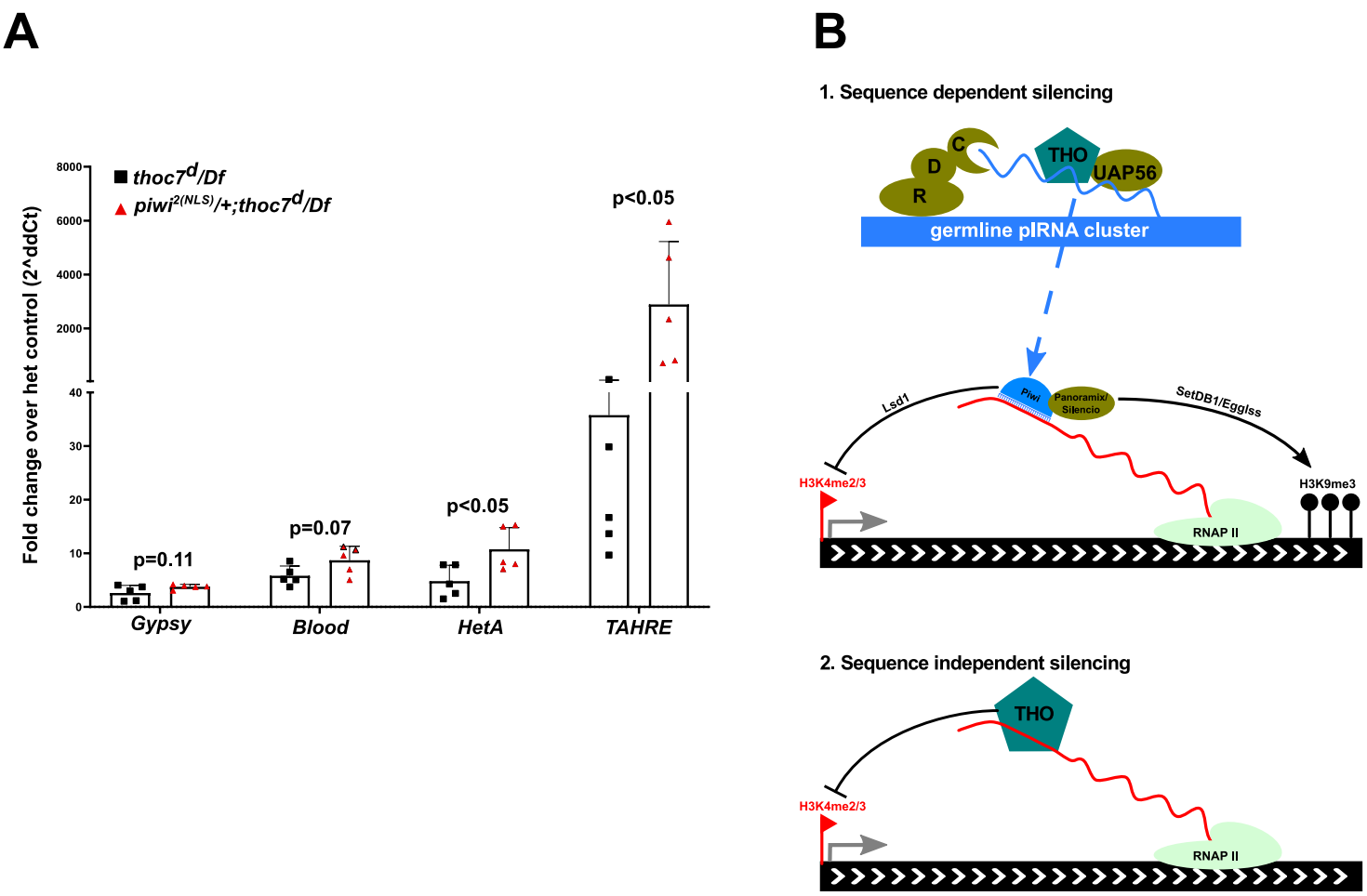

Figure S6. *piwi* and *thoc7* mutants genetic interaction in transposon silencing, and sequence-specific and sequence-independent transposon silencing. Related to Figure 7.

A. RT-qPCR measure *Gypsy*, *Blood*, *HeT-A* and *THARE* expression in the indicated genotype. $2^{-\Delta\Delta Ct}$ is used to calculate relative fold expression change over heterozygous control after normalization to *rp49*. The p value is calculated by *t* test from five replicates.

B. We propose that two independent mechanisms silence transposons in *Drosophila* ovaries. 1) The Piwi-piRNA pathway provides sequence specific transposon recognition for transcriptional silencing, which represents "adaptive" genome immunity, which is gained following invasion of a novel mobile element. THO mediated piRNA biogenesis fuels Piwi mediated silencing pathway. 2) Additionally, the THO complex provides sequence-independent "adaptive or innate" transposon silencing. We speculated that inefficient splicing, which is common to transposon families, is recognized by THO complex.

Table S1: qPCR primer sequences. Related to STAR Methods:

Target	Sequences
rp49	CCG CTT CAA GGG ACA GTA TCT G ATC TCG CCG CAG TAA ACG C
sj	AAC AGC TCC TCG CCC TTG TGAGTCAGACCTCGAAATCGT
GFP1	GACGTAAACGGCCACAAGTT GTAGGTCAGGGTGGTCACGA
GFP2	CGA CAA CCA CTA CCT GAG CA CCATGCCGAGAGTGATCC
Gypsy	CTT CAC GTT CTG CGA GCG GTC T CGC TCG AAG GTT ACC AGG TAG GTT C
Blood	CCA ACA AAG AGG CAA GAC CG TCG AGC TGC TTA CGC ATA CTG TC
HeT-A	CGC GCG GAA CCC ATC TTC AGA CGC CGC AGT CGT TTG GTG AGT
TAHRE	CTG TTG CAC AAA GCC AAG AA GTT GGT AAT GTT CGC GTC CT